Morphology for Hexagonal Image Processing

Taner CEVIK (taner.cevik@nisantasi.edu.tr)
Nisantasi University
Sajjad NEMATZADEH
Nisantasi University
Nazife CEVIK
Istanbul Arel University
Mahsa Torkamanian AFSHAR
Nisantasi University

Research Article

Keywords: Hexagonal Image Processing, Morphology, Dilation, Erosion, Opening, Closing, Image Analysis

Posted Date: April 11th, 2022

DOI: https://doi.org/10.21203/rs.3.rs-1537955/v1

Morphology for Hexagonal Image Processing

Taner CEVIK[1, *], Sajjad NEMATZADEH[1], Nazife CEVIK[2], Mahsa Torkamanian AFSHAR[1]

[1] Department of Computer Engineering, Nisantasi University, Istanbul, Turkey
[2] Department of Computer Engineering, Istanbul Arel University, Istanbul, Turkey

* Corresponding author, email: taner.cevik@nisantasi.edu.tr

Abstract

Morphological operators for binary and grayscale images are commonly used to eliminate noise, recognize contours or specific structures, and arrange shapes in image processing. Even though morphology has been substantially developed in square-pixel-based-image-processing (SIP), no effort has been made to construct morphological operators in hexagonal-pixel-based-image-processing (HIP) yet. In this paper, we transform basic SIP-domain-morphological operators such as dilation, erosion, closing, and opening into HIP-domain and compare their performance with their SIP counterparts, taking into account 65 similarity- dissimilarity metrics for binary and four metrics for grey-scale proposed so far in the literature. It is the first time to give the fundamental morphological operators in the HIP domain. The operators developed in this paper initiate the research about morphology in the HIP domain by successfully filling a significant gap by eliminating HIP's lack of basic operators.

Keywords: Hexagonal Image Processing, Morphology, Dilation, Erosion, Opening, Closing, Image Analysis.

1. Introduction

The art of replicating human vision and converting it to computer vision is image processing. Indeed, the data in the light physical medium is continuous, and this continuous data is obtained using specific sensors. These sensors are utilized in square or rectangular arrays and differ in the light spectrum to which they are sensitive. Computers can only process digital data, even though light data is continuous. Continuous light data must therefore be sampled and digitized. Because square or rectangular sensor arrays are employed, downstream computer processing is developed accordingly. As a result, the smallest data unit of digitized data in a computer environment, the pixel, is built as a square. However, sampling light data on a hexagonal lattice and then processing it as a hexagon domain can change many things and produce promising results. For decades, hexagonal geometry has been studied. It was assumed until Hales [1], [2] proved otherwise that hexagons were the most significant way to split a plane into areas of equal area. Honeycombs are another natural hexagonal encounter with hexagonal geometry, in addition to the natural hexagonal arrangement of photoreceptors in the fovea [3].

The use of hexagonal pixels for picture capture is a more recent innovation in hexagonal image processing. The hexagonal lattice construction has several advantages over its square counterpart. More excellent radial symmetry permits the application of circular symmetric kernels, which improves detection accuracy for both straight and curved edges and the homogeneity of the hexagonal lattice format, which gives local equality and uniqueness [4], [5].

A collection of operations on Euclidean space for quantitative description of geometrical structures has been proposed as mathematical morphology [6]. The set theory supports mathematical analysis, integral geometry, and lattice algebra. In recent years, mathematical morphology is becoming crucial in image processing and

computer vision applications. The development of MM is characterized by cross-fertilization between applications, methodologies, theories, and algorithms. It leads to several processing tools to image filtering, image segmentation and classification, image measurements, pattern recognition, or texture analysis and synthesis [7]. In industrial vision applications, mathematical morphology can be used to implement fast object recognition [8]–[10], image segmentation [11], [12], and industrial inspection [13]–[15].

The principles of mathematical morphology and its applications were first developed systematically by Matheron [16] and Serra [17], [18]. Further applications for signal and image processing were presented by Giardina and Dougherty [19], followed by the tutorial papers of Haralick [20] and Maragos [21]. Extending the theory to gray-scale images was done by Stemberg [22], [23], and Serra [17].

1.1. Contribution of this work - Despite its significant advantages, the hexagonal grid has not been widely used in computer vision and graphics until recently. The fundamental issue limiting the usage of the hexagonal picture structure is a lack of hardware for capturing and displaying hexagon-based images. Various attempts have mimicked hexagonal grids using regular rectangular grid technology. Simulation techniques include rectangular pixels, pseudo-hexagonal pixels, simulated hexagonal pixels, and virtual hexagonal pixels. While none of these simulation approaches can fully demonstrate the benefits of a proper hexagonal structure, their use provides us with practical tools for image processing on hexagonal grids. It allows us to continue our theoretical research into hexagonal structures in modern computer vision and graphics systems [24].

So far, no morphology studies have been performed in the HIP domain, and the most basic operations such as dilation and erosion have not been suggested on how to do it in the hexagonal domain. In mathematical morphology, the basic operations are dilation and erosion, combined to form other operations like opening and closing [14]. The kernel utilized in a morphological operation is the Structuring Element (SE). This study develops the HIP counterparts of these primary SIP morphological operations. The most basic SE is a straight line with an arbitrary length, either vertically or horizontally. Other more complex SEs can be easily derived from these straight-line SEs. The directions of these straight-line SEs on the SIP domain are mainly 0°, 45° 90°, 135° while they are mainly 0°, 60° and 120° on the HIP domain. The article proposes these primary straight-length SEs on the HIP domain. While implementing morphology on the HIP domain firstly, the results of the morphological operations are carefully analysed by taking into 65 similarity and dissimilarity metrics that have been proposed in the literature so far.

1.2. Organization of the article – This article is categorized as follows: Section 2 gives a brief introduction to the fundamentals of the HIP. Section 3 describes the principles of mathematical morphology. Section 4 presents the HIP equivalents of the essential SIP morphological operations. Section 5 introduces the dataset used for the testing, the experimental setup, and the 68 similarity- dissimilarity metrics for binary and four metrics for grey-scale that are taken into account and the discussions of the results achieved. Finally, Section IV states the conclusions we have drawn and the possible future directions of our research.

2. Fundamentals of HIP

The digital images in the HIP domain contain regular hexagonal cells (Hexel), which correspond to the concept of the pixel in SIP. Due to their unique characteristics, hexels may be a viable alternative for conveying visual data. In an ideal scenario, a hexel-supported-camera-sensor should provide an excellent physical infrastructure to extract intensity and color information and display it on a hexel-supported-monitor. Few goods are publicly available at the time of authoring this article. As a result, we used mimic procedures to convert pixels to hexels. The differences in coordinate systems of SIP and HIP drove us to create a mechanism to project pixels on hexels. Figure 1 demonstrates the relations between cells and their neighbors. Hexels of upper and lower rows are calculated by averaging the corresponding pixels. Other values are copied directly.

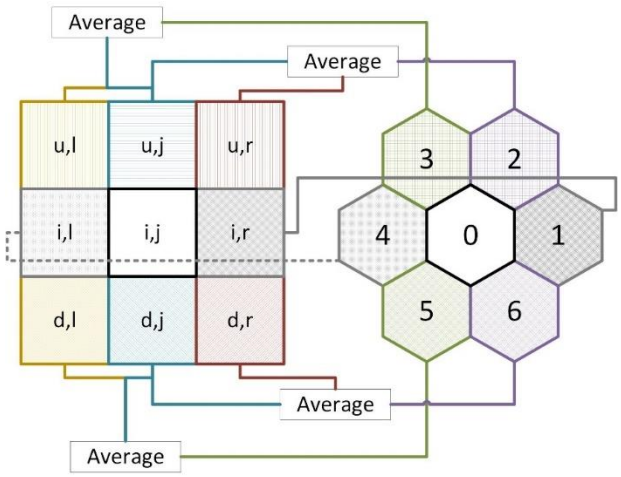

Figure 1. Identifying neighbors of a hexel using the pixel counterpart.

Pseudocode1 (MATLAB function) gives the algorithm of image projection from SIP to HIP. This algorithm duplicates boundary pixels and copies at the edges of an image. Also, to better understand, a structure of data containing the hexel and its neighbors is returned.

Pseudocode1. Converting SIP image into the HIP image

```
function [hexagonsPadded] = imageConvertHexPaddedRep(hexagonsPadded, f)
 num_rows=size(f,1);
 num_cols=size(f,2);
 for i = 1:num_rows
   for j = 1:num_cols
           gryval = f(i,j);
           r =min (xind+1, num_cols);
           l =max (xind-1,1);
           u =max (yind-1,1);
           d =min (yind+1, num_rows);

           ngb1=f(i,r);
           ngb2=(f(u,r)+f(u,j))/2.0;
           ngb3=(f(u,l)+f(u,j))/2.0;
           ngb4=f(i,l);
           ngb5=(f(d,l)+f(d,j))/2.0;
           ngb6=(f(d,r)+f(d,j))/2.0;
           hexagonsPadded(i,j) = struct('grayvalue', gryval, 'xindex', i, 'yindex', j, 'ngb1', ngb1,  'ngb2', ngb2,   'ngb3', ngb3, 'ngb4',
           ngb4, 'ngb5', ngb5, 'ngb6', ngb6);
   end
 end
```

Although the data structure of the HIP mentioned in pseudocode 1 may suffer from memory and process inefficiency, it gives an evident and comprehendible infrastructure to pursue the morphology and other relevant operations. Finally, the memory and process-friendly versions of these operations can be coded. The following sections explain the fundamental concepts of morphology customized for hexagonal systems.

3. Mathematical Morphology

A set of pixels can be used to represent an image. Working with two images is how morphological operators can be visualized. The active image is the one that is being processed, and the other image, which is the kernel

or so-called nonlinear filter, is referred to as the configuration element [25]. G. Matheron and J. Serra established a family of nonlinear filters called mathematical morphology in their mineralogical work in the early 1960s [26], [27]. Each configuration element has a unique design that acts as a probe or filter for the active image. The geometry of the configuration element determines the filter's effect on the image. All morphological filters combine two basic operators, erosion and expansion. The mathematical morphology was later generalized to the case of grayscale images [28], [29], whereas the original theory was considered for binary images.

3.1. Binary morphology

Pixels are added to a configuration element when it touches at least one pixel during the dilation process, expanding the item. The term dilation has a different meaning in different places. For instance, if each point a of A is a seed that produces the flower B, the union of all the flowers is the dilation of A by B (by placing the origin of B at every a). Isotropic expansion techniques are commonly used in binary image processing, and dilation by disk structuring components corresponds to them. The *8-neighborhood* operation of dilation by a small square ($3x3$), often known as "fill," "expand," or "grow," is easily achieved using adjacently connected array designs. Dilation increases the visibility of an object by filling small gaps in it. Equation (1) defines the dilation of the binary image A caused by configuring element B [14].

$$A \oplus_b B = \{c \in E^N | c = a + b \; for \; some \; a \in A \; and \; b \in B\} \quad (1)$$

where E^N is the set of all points $p = (x_1, x_2, \ldots, x_N)$ in N-dimension Euclidean space, whilst A and B are subsets of E^N.

Properties of the dilation operation are:

Commutative	$A \oplus_b B = B \oplus_b A$
Associative	$A \oplus_b (B \oplus_b C) = (A \oplus_b B) \oplus_b C)$
Translation invariance	$(A)_x \oplus_b B = (A \oplus_b B)_x$
Increasing	If A⊆B, then $A \oplus_b D \subseteq B \oplus_b D$
Distributive	$(A \cap B) \oplus_b C \subseteq (A \oplus_b C) \cap (B \oplus_b C)$ $(A \cup B) \oplus_b C = (A \oplus_b C) \cup (B \oplus_b C)$

The morphological dual of dilation is erosion. It combines two sets by subtracting set components using vector subtraction. When a configuration element comes into touch with at least one pixel during the erosion process, pixels are eliminated, effectively shrinking the image's objects. Erosion does not have the feature of commutativity. The locus of all centers c can be read as the erosion of A by B, with the translation B wholly contained within the set A. The object's size is reduced through erosion until only the most durable remains. The erosion of a binary image A by structuring element B is represented by Equation (2) [14].

$$A \ominus_b B = \{x \in E^N | x + b \; \in A \; for \; every \; b \in B\} \quad (2)$$

Properties of the dilation operation are:

Non-commutative	$A \ominus_b B \neq B \ominus_b A$
Associative	$A \ominus_b (B \ominus_b C) = (A \ominus_b B) \ominus_b C)$

Translation invariance	$(A)_x \ominus_b B = (A \ominus_b B)_x$
Increasing	If A⊆B, then $A \ominus_b D \subseteq B \ominus_b D$
Distributive	$(A \cap B) \ominus_b C = (A \ominus_b C) \cap (B \oplus_b C)$ $(A \cup B) \ominus_b C \supseteq (A \ominus_b C) \cup (B \ominus_b C)$

As a result of combining the dilation and erosion operations, we may create several composite morphological filters. The opening and closing operations, which are defined as the sequences of erosion-dilation and dilation-erosion, respectively (Equations (3-4)), are the most common composite operators [30]:

$$A \circ B = (A \ominus B) \oplus B \quad (3)$$

$$A \bullet B = (A \oplus B) \ominus B \quad (4)$$

Idempotency is the primary property of the opening and closing operations. That is, the image does not change any more when the open and close operations with the same structuring element are repeated. Equations 5 and 6 performs this operation.

$$A \circ B \circ B = A \circ B \quad (5)$$

$$A \bullet B \bullet B = A \bullet B \quad (6)$$

Figure 2 shows the primary structuring elements used in dilation and erosion, while Figure 3 depicts the results of the dilation, erosion, opening, and closing operations by applying the primary SEs given in Figure 2.

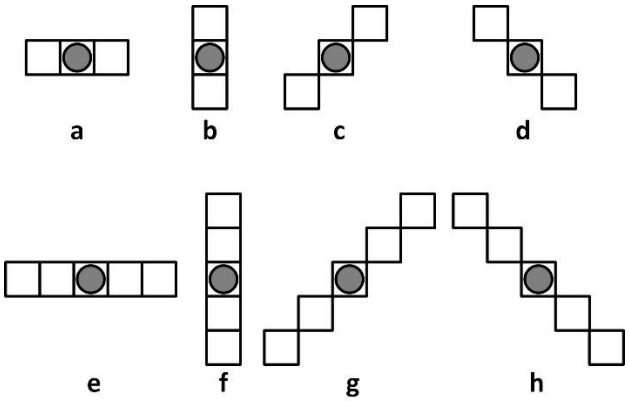

Figure 2. Basic structuring elements used in dilation and erosion. (a) $SE_{0°, L=3}$, (b) $SE_{90°, L=3}$, (c) $SE_{45°, L=3}$, (d) $SE_{135°, L=3}$, (e) $SE_{0°, L=5}$, (f) $SE_{90°, L=5}$, (g) $SE_{45°, L=5}$, (h) $SE_{135°, L=5}$.

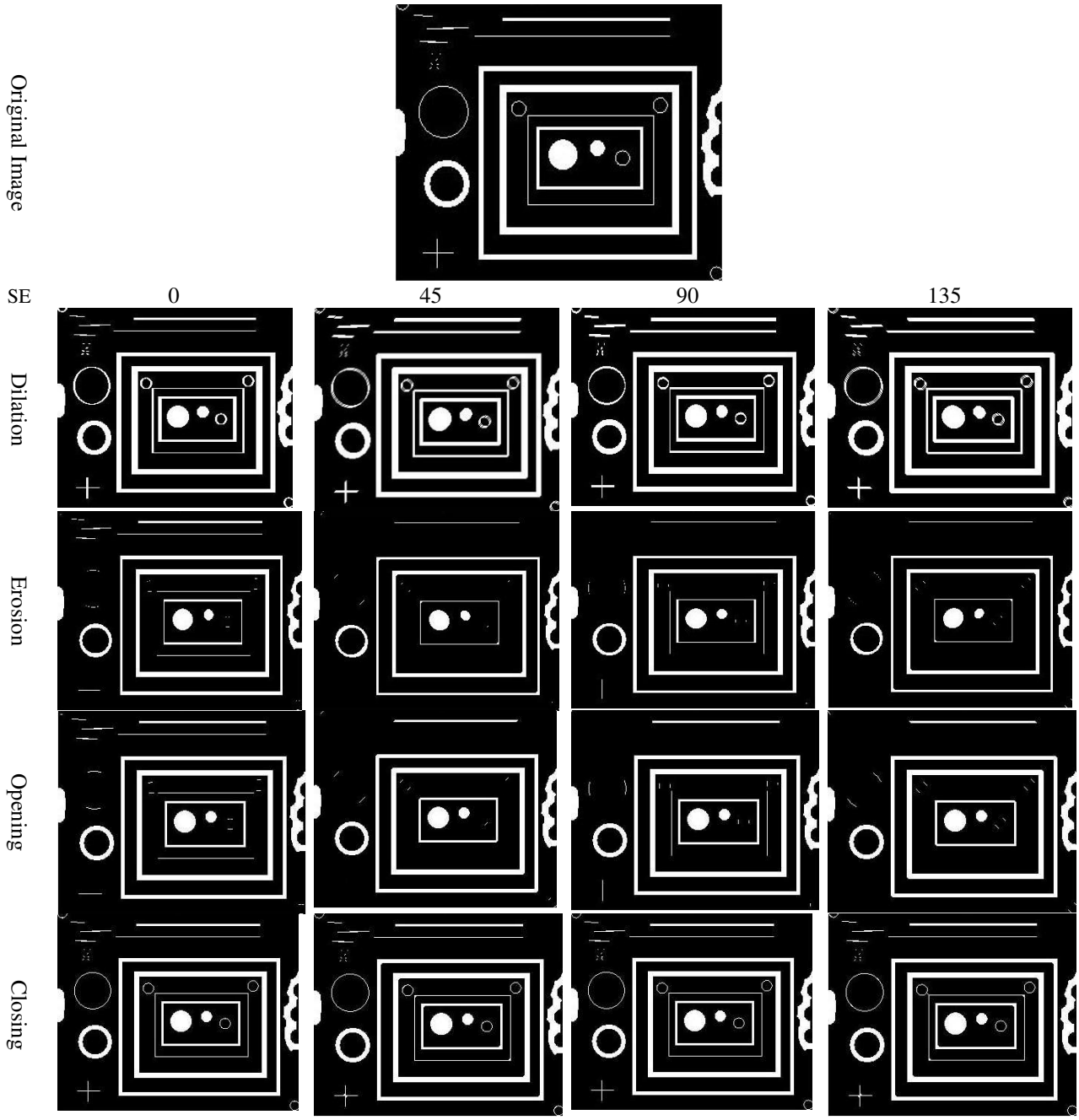

Figure 3. Results of the dilation, erosion, opening and closing operations by applying the basic SEs given in Figure 2.

3.2. Gray-scale morphology

A grayscale image is a three-dimensional set with the first two elements being the pixel's x and y coordinates and the third element being the grayscale value. Binary morphology can easily be stretched to grayscale morphology. The main differences come from the definitions of dilation and erosion, which are essential in other procedures. Logic operations are transformed into mathematical equivalents. In most circumstances, grayscale morphology is often limited to plane structural elements, resulting in simple dilation and erosion procedures using Min and Max functions [31], [32]. The dilation and erosion of a gray-scale image f by the structuring element s are respectively given in Equations 7 and 8.

$$f \oplus s = max\{(f)_p | p \in s\} = \underset{p \in s}{max}(f)_p \quad (7)$$

$$f \ominus s = min\{(f)_p | p \in s\} = \underset{p \in s}{min}(f)_p \quad (8)$$

With this concept, the gray-scale opening and closing operations are defined in Equations 9 and 10.

$$f \circ s = \underset{(a \in s)}{max} \underset{(b \in s)}{min} f(x - a + b) \quad (9)$$

$$f \bullet s = \underset{(a \in s)}{min} \underset{(b \in s)}{max} f(x - a + b) \quad (10)$$

Figure 4 illustrate the results of the dilation, erosion, opening and closing operations on a gray-scale image by applying the basic SEs given in Figure 2.

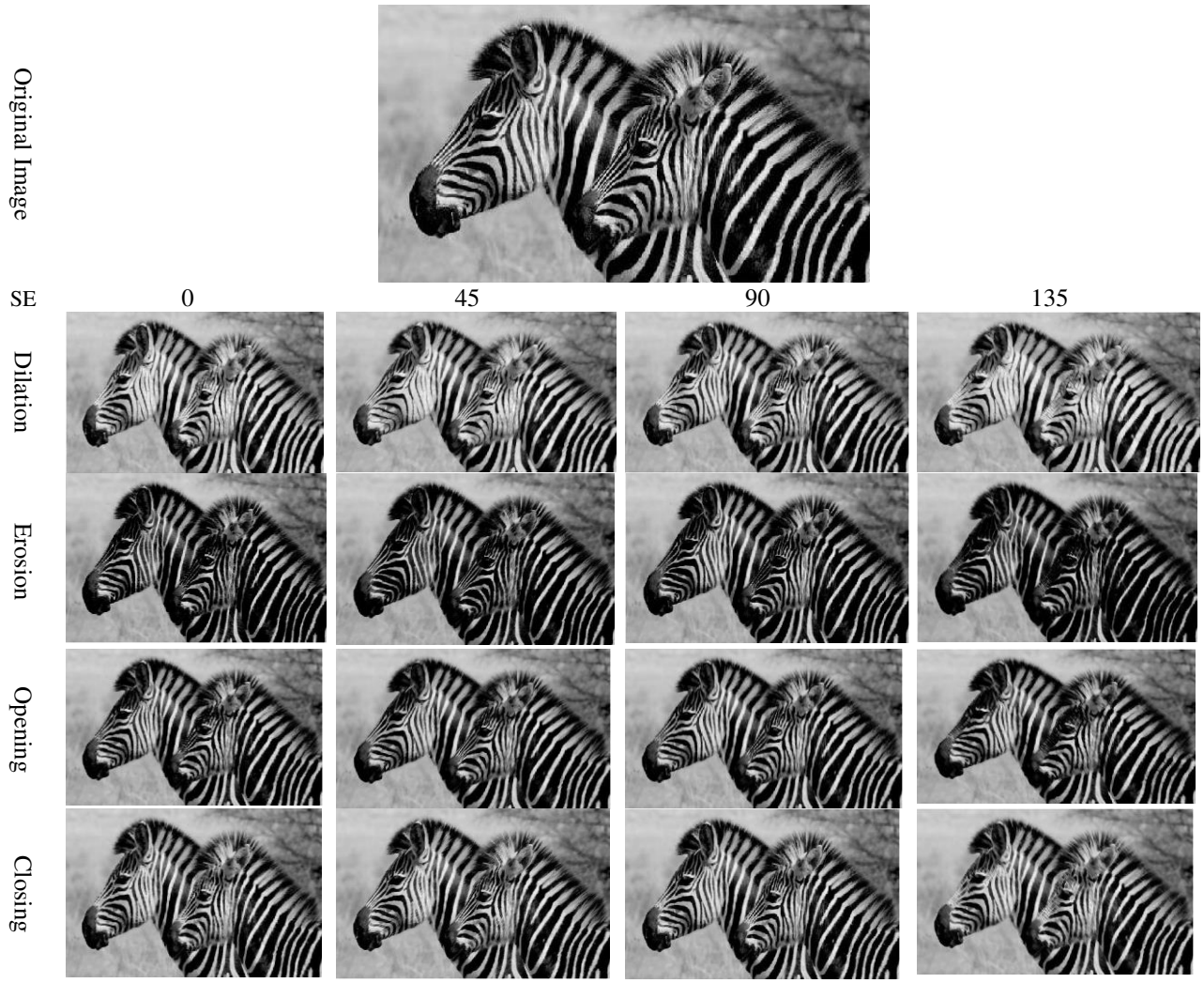

Figure 4. Results of the gray-scale dilation, erosion, opening, and closing operations by applying the basic SEs given in Figure 2.

4. Morphology for HIP

Since morphology is used in various fields of image processing such as image filtering, image segmentation, and classification, image measurements, pattern recognition, or texture analysis and synthesis, the definition of morphology in the HIP will fill a critical deficiency. Whereas in the classical SIP domain, there are 4-links or 8-links between each pixel and neighboring pixels, there are only six in HIP. Furthermore, based on these neighborhoods, SIP has 4 major angular directions, 0°, 45°, 90°, and 135°, while HIP has 3 angular directions, 0°, 60°, and 120°. Because of these structural differences, the basic SEs defined in SIP need to be redefined in HIP. To better express the relationships between pixels and their calculations, neighborhood-based indexing representation is preferred rather than ordinary numerical indexing, as illustrated in Figure 5.

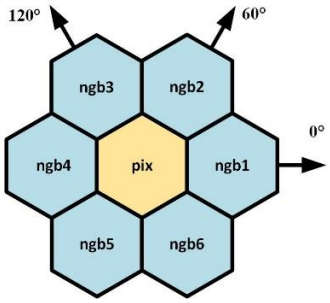

Figure 5. Representation of the 1-hop-neighborhood-based indexing in HIP.

Based on this structure, 1-tier correspondents of the basic binary SEs illustrated in Figure 2 are depicted in Figure 6.

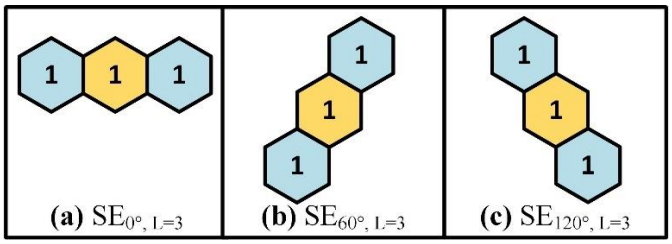

Figure 6. HIP 1- tier correspondents of the basic binary SEs that are illustrated in Figure 1.

Algebra is not defined for HIP; for example, there is no corresponding matrix or convolution operator. Thus, all matrix-based algebraic operations are performed individually, pixel by pixel. Dilation and erosion operations in the HIP domain for the 1-tier architecture is performed as Equations 11-16.

$$f_p \oplus seHex_{0°,L=3} = \left(p.ngb4 \vee seHex_{0°,L=3_{-1}}\right) \vee (p \vee seHex_{0°,L=3_0}) \vee \left(p.ngb1 \vee seHex_{0°,L=3_{+1}}\right) \quad (11)$$

$$f_p \oplus seHex_{60°,L=3} = \left(p.ngb5 \vee seHex_{60°,L=3_{-1}}\right) \vee (p \vee seHex_{60°,L=3_0}) \vee \left(p.ngb2 \vee seHex_{60°,L=3_{+1}}\right) \quad (12)$$

$$f_p \oplus seHex_{120°,L=3} = \left(p.ngb5 \vee seHex_{120°,L=3_{-1}}\right) \vee (p \vee seHex_{120°,L=3_0}) \vee \left(p.ngb2 \vee seHex_{120°,L=3_{+1}}\right) \quad (13)$$

$$f_p \ominus seHex_{0°,L=3} = \left(p.ngb4 \wedge seHex_{0°,L=3_{-1}}\right) \wedge (p \wedge seHex_{0°,L=3_0}) \wedge \left(p.ngb1 \wedge seHex_{0°,L=3_{+1}}\right) \quad (14)$$

$$f_p \ominus seHex_{60°,L=3} = \left(p.ngb5 \wedge seHex_{60°,L=3_{-1}}\right) \wedge (p \wedge seHex_{60°,L=3_0}) \wedge \left(p.ngb2 \wedge seHex_{60°,L=3_{+1}}\right) \quad (15)$$

$$f_p \ominus seHex_{120°,L=3} = \left(p.ngb5 \wedge seHex_{120°,L=3_{-1}}\right) \wedge (p \wedge seHex_{120°,L=3_0}) \wedge \left(p.ngb2 \wedge seHex_{120°,L=3_{+1}}\right) \quad (16)$$

With the same logic, the 1- tier opening and closing operations in the HIP are implemented in Equations 17-22.

$$f_p \circ seHex_{0°,L=3} = (f_p \ominus seHex_{0°,L=3}) \oplus seHex_{0°,L=3} \quad (17)$$
$$f_p \bullet seHex_{0°,L=3} = (f_p \oplus seHex_{0°,L=3}) \ominus seHex_{0°,L=3} \quad (18)$$
$$f_p \circ seHex_{60°,L=3} = (f_p \ominus seHex_{60°,L=3}) \oplus seHex_{60°,L=3} \quad (19)$$
$$f_p \bullet seHex_{60°,L=3} = (f_p \oplus seHex_{60°,L=3}) \ominus seHex_{60°,L=3} \quad (20)$$
$$f_p \circ seHex_{120°,L=3} = (f_p \ominus seHex_{120°,L=3}) \oplus seHex_{120°,L=3} \quad (21)$$
$$f_p \bullet seHex_{120°,L=3} = (f_p \oplus seHex_{120°,L=3}) \ominus seHex_{120°,L=3} \quad (22)$$

The same reasoning applies to morphologic operations involving lengthier or larger structural elements, but the processes taken are naturally more complicated. Pixels' connectivity and neighborhood arrangement for the 2-tier architecture are shown in Figure 7.

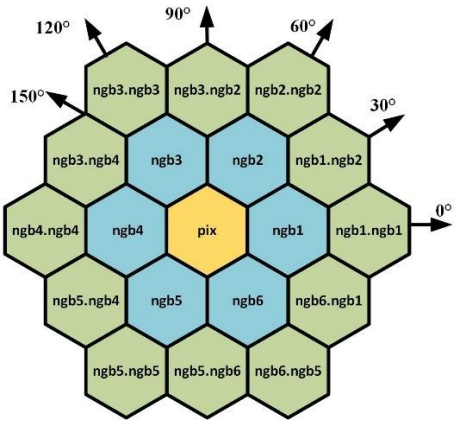

Figure 7. Representation of the 2-hop-neighborhood-based indexing in HIP.

Based on this structure, 2-tier correspondents of the primary SIP SEs illustrated in Figure 2 are depicted in Figure 8.

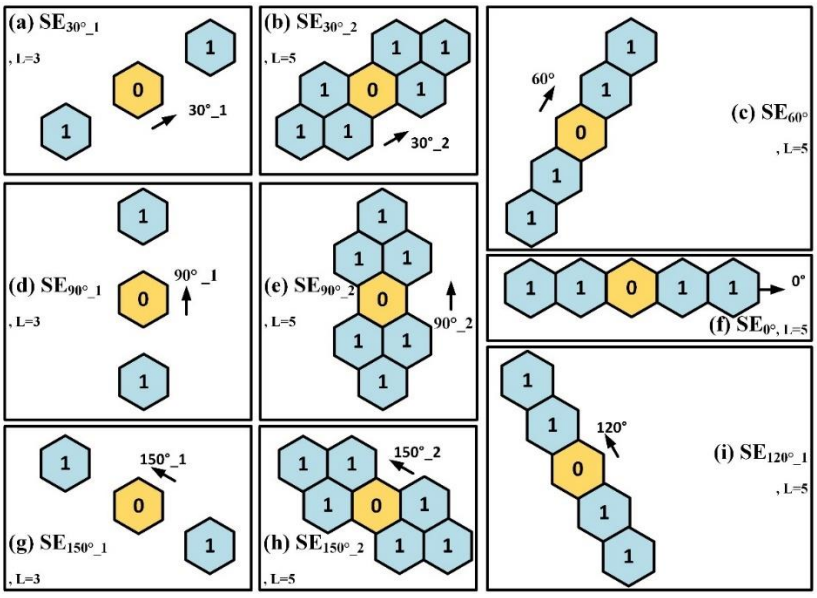

Figure 8. HIP 2-tier correspondents of the basic SEs that are illustrated in Figure 1.

Dilation and erosion operations in HIP domain for the 2-tier architecture is performed in Equations 23-31.

$$f_p \oplus seHex_{0°,L=5} = \left(p.ngb4.ngb4 \vee seHex_{0°,L=5_{-2}}\right) \vee \left(p.ngb4 \vee seHex_{0°,L=5_{-1}}\right) \vee (p \vee seHex_{0°,L=5_0}) \vee \left(p.ngb1 \vee seHex_{0°,L=5_{+1}}\right) \vee \left(p.ngb1.ngb1 \vee seHex_{0°,L=5_{+2}}\right) \quad (23)$$

$$f_p \oplus seHex_{30°\_1,L=3} = \left(p.ngb5.ngb4 \vee seHex_{30°\_1,L=3_{-1}}\right) \vee (p \vee seHex_{30°\_1,L=3_0}) \vee \left(p.ngb1.ngb2 \vee seHex_{30°\_1,L=3_{+1}}\right) \quad (24)$$

$$f_p \oplus seHex_{30°\_2,L=5} = \left(p.ngb5.ngb4 \vee seHex_{30°\_2,L=5_{-2}}\right) \vee \left(p.ngb4 \vee seHex_{30°\_2,L=5_{-1,-1}}\right) \vee \left(p.ngb5 \vee seHex_{30°\_2,L=5_{-1,+1}}\right) \vee (p \vee seHex_{30°\_2,L=5_0}) \vee \left(p.ngb2 \vee seHex_{30°\_2,L=5_{+1,-1}}\right) \vee \left(p.ngb1 \vee seHex_{30°\_2,L=5_{+1,+1}}\right) \vee \left(p.ngb1.ngb2 \vee seHex_{30°\_2,L=5_{+2}}\right) \quad (25)$$

$$f_p \oplus seHex_{60°,L=5} = \left(p.ngb5.ngb5 \vee seHex_{60°,L=5_{-2}}\right) \vee \left(p.ngb5 \vee seHex_{60°,L=5_{-1}}\right) \vee (p \vee seHex_{60°,L=5_0}) \vee \left(p.ngb2 \vee seHex_{60°,L=5_{+1}}\right) \vee \left(p.ngb2.ngb2 \vee seHex_{60°,L=5_{+2}}\right) \quad (26)$$

$$f_p \oplus seHex_{90°\_1,L=3} = \left(p.ngb5.ngb6 \vee seHex_{90°\_1,L=3_{-1}}\right) \vee (p \vee seHex_{90°\_1,L=3_0}) \vee \left(p.ngb3.ngb2 \vee seHex_{90°\_1,L=3_{+1}}\right) \quad (27)$$

$$f_p \oplus seHex_{90°_2,L=5} = \left(p.ngb5.ngb6 \vee seHex_{90°_2,L=5_{-2}}\right) \vee \left(p.ngb5 \vee seHex_{90°_2,L=5_{-1,-1}}\right) \vee \left(p.ngb6 \vee seHex_{90°_2,L=5_{-1,+1}}\right) \vee (p \vee seHex_{90°\_2,L=5_0}) \vee \left(p.ngb3 \vee seHex_{90°\_2,L=5_{+1,-1}}\right) \vee \left(p.ngb2 \vee seHex_{90°\_2,L=5_{+1,+1}}\right) \vee \left(p.ngb3.ngb2 \vee seHex_{90°\_2,L=5_{+2}}\right) \quad (28)$$

$$f_p \oplus seHex_{120°,L=5} = \left(p.ngb6.ngb5 \vee seHex_{120°,L=5_{-2}}\right) \vee \left(p.ngb6 \vee seHex_{120°,L=5_{-1}}\right) \vee \left(p \vee seHex_{120°,L=5_0}\right) \vee \left(p.ngb3 \vee seHex_{120°,L=5_{+1}}\right) \vee \left(p.ngb3.ngb3 \vee seHex_{120°,L=5_{+2}}\right) \quad (29)$$

$$f_p \oplus seHex_{150°\_1,L=3} = \left(p.ngb6.ngb1 \vee seHex_{150°\_1,L=3_{-1}}\right) \vee (p \vee seHex_{150°\_1,L=3_0}) \vee \left(p.ngb3.ngb4 \vee seHex_{150°\_1,L=3_{+1}}\right) \quad (30)$$

$$f_p \oplus seHex_{150°\_2,L=5} = \left(p.ngb6.ngb1 \vee seHex_{150°\_2,L=5_{-2}}\right) \vee \left(p.ngb6 \vee seHex_{150°\_2,L=5_{-1,-1}}\right) \vee \left(p.ngb1 \vee seHex_{150°\_2,L=5_{-1,+1}}\right) \vee (p \vee seHex_{150°\_2,L=5_0}) \vee \left(p.ngb4 \vee seHex_{150°\_2,L=5_{+1,-1}}\right) \vee \left(p.ngb3 \vee seHex_{150°\_2,L=5_{+1,+1}}\right) \vee \left(p.ngb3.ngb4 \vee seHex_{150°\_2,L=5_{+2}}\right) \quad (31)$$

The 2- tier opening and closing operations in HIP are implemented using Equations 32-49.

$$f_p \circ seHex_{0°,L=5} = (f_p \ominus seHex_{0°,L=5}) \oplus seHex_{0°,L=5} \quad (32)$$
$$f_p \bullet seHex_{0°,L=3} = (f_p \oplus seHex_{0°,L=5}) \ominus seHex_{0°,L=5} \quad (33)$$
$$f_p \circ seHex_{30°\_1,L=3} = (f_p \ominus seHex_{30°\_1,L=3}) \oplus seHex_{30°\_1,L=3} \quad (34)$$
$$f_p \bullet seHex_{30°\_1,L=3} = (f_p \oplus seHex_{30°\_1,L=3}) \ominus seHex_{30°\_1,L=3} \quad (35)$$
$$f_p \circ seHex_{30°\_2,L=5} = (f_p \ominus seHex_{30°\_2,L=5}) \oplus seHex_{30°\_2,L=5} \quad (36)$$
$$f_p \bullet seHex_{30°\_2,L=5} = (f_p \oplus seHex_{30°\_2,L=5}) \ominus seHex_{30°\_2,L=5} \quad (37)$$
$$f_p \bullet seHex_{60°,L=5} = (f_p \oplus seHex_{60°,L=5}) \ominus seHex_{60°,L=5} \quad (38)$$
$$f_p \circ seHex_{60°,L=5} = (f_p \ominus seHex_{60°,L=5}) \oplus seHex_{60°,L=5} \quad (39)$$
$$f_p \circ seHex_{90°\_1,L=3} = (f_p \ominus seHex_{90°\_1,L=3}) \oplus seHex_{90°\_1,L=3} \quad (40)$$
$$f_p \bullet seHex_{90°\_1,L=3} = (f_p \oplus seHex_{90°\_1,L=3}) \ominus seHex_{90°\_1,L=3} \quad (41)$$
$$f_p \circ seHex_{90°\_2,L=5} = (f_p \ominus seHex_{90°\_2,L=5}) \oplus seHex_{90°\_2,L=5} \quad (42)$$
$$f_p \bullet seHex_{90°\_2,L=5} = (f_p \oplus seHex_{90°\_2,L=5}) \ominus seHex_{90°\_2,L=5} \quad (43)$$
$$f_p \circ seHex_{120°,L=5} = (f_p \ominus seHex_{120°,L=5}) \oplus seHex_{120°,L=5} \quad (44)$$
$$f_p \bullet seHex_{120°,L=5} = (f_p \oplus seHex_{120°,L=5}) \ominus seHex_{120°,L=5} \quad (45)$$
$$f_p \circ seHex_{150°\_1,L=3} = (f_p \ominus seHex_{150°\_1,L=3}) \oplus seHex_{150°\_1,L=3} \quad (46)$$
$$f_p \bullet seHex_{150°\_1,L=3} = (f_p \oplus seHex_{150°\_1,L=3}) \ominus seHex_{150°\_1,L=3} \quad (47)$$
$$f_p \circ seHex_{150°\_2,L=5} = (f_p \ominus seHex_{150°\_2,L=5}) \oplus seHex_{150°\_2,L=5} \quad (48)$$
$$f_p \bullet seHex_{150°\_2,L=5} = (f_p \oplus seHex_{150°\_2,L=5}) \ominus seHex_{150°\_2,L=5} \quad (49)$$

In the following section, we present the results of the basic morphological operations that are implemented on the HIP domain. Besides, the images formed by morphology are compared with the original images. Also,

similarity and dissimilarity analyses are performed, and the results are compared with their conjugates in the SIP domain.

5. Experimental Results

The experimental analysis is performed on the Barcelona Images for Perceptual Edge Detection (BIPED) Dataset [33] contains 250 high-definition outdoor images of 1280x720 pixels each. The dataset includes both the colored images and their edge maps called ground-truths. An example-colored image and its edge-map are shown in Figure 9.

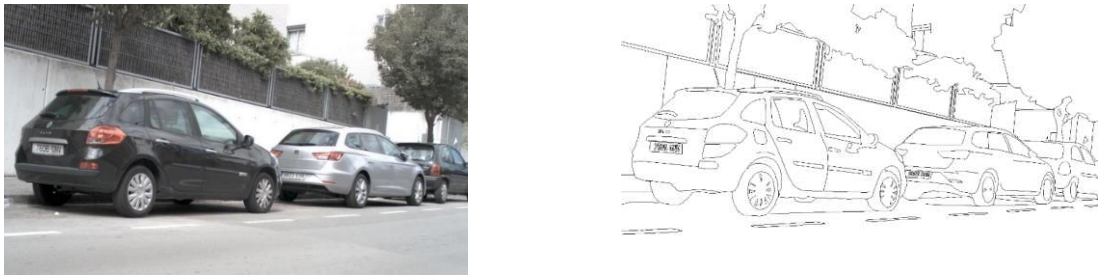

(a) Original Image (b) Edge-map

Figure 9. An example-colored image and its edge-map from BIDEP dataset.

Morphology operations are performed in both domains as grayscale and binary. SIP-morphology is implemented on the original images, while HIP-morphology is applied on the HIP-converted versions. Therefore, before applying the HIP morphology, all images in the dataset are first converted to grayscale, and then both grayscale and binary edge maps are transferred to the HIP domain. Figure 11 illustrates the entire methodology and the individual steps implemented.

After processing images using the morphology implementation, the results are analyzed for similarity and dissimilarity between the SIP and HIP-domain-processed images and the originals. For similarity-dissimilarity performance analysis of binary-morphology-implementation, 68 different metrics [34] that are listed in Table 1 are considered. For similarity-dissimilarity performance analysis of gray-scale-morphology-implementation, four benchmark metrics shown in Table2 are taken into account.

TABLE 1. Evaluation metrics for similarity-dissimilarity performance analysis of binary-morphology-implementation.

Similarity			Dissimilarity
AMPLE (Analyzing Method Patterns to Locate Errors) [35]	fossum [36]	Pmsc (Pearson 1 coefficient of mean square contingency) [37], [38]	baulieu [39]
Anderberg [40]	gini (Gini coefficient) [41]	RT (Rogers and Tanimoto) [42]	Beuc (Binary euclidean distance) [43]
BB (Braun and Blanquet) [44]	GK1 (Goodman and Kruskal 1) [45],[48]	scott [49]	BLWMN (Binary Lance and Williams nonmetric) [50]
BUB 1,2 (Baroni-Urbani-Buser 1,2) [51]	GKlambda (Goodman and Kruskal's lambda) [45]–[48]	SM (Sokal and Michener) [52]	BSeuc (Binary squared euclidean distance) [53]
CK (Cohen's kappa) [54]	goodall (Goodall coefficient) [55]	soergel (Soergel distance) [56]	Bshape (Binary shape) [57]
cole [58]	hamann (Hamann coefficient) [59]	sorensen [60]	chord (Chord distance) [61]
dennis (Dennis M4) [62]	HD (Hawkins and Dotson coefficient) [63]	sorgenfrei (Sorgenfrei coefficient) [64]	GK 2-4 (Goodman and Kruskal 2-4) [45]–[48]
dice [65]	jaccard [66], [67]	SS 1-5 (Sokal and Sneath 1-5) [68], [69]	Gktau (Goodman and Kruskal's tau) [45]–[48]
diceasym1 (Dice asymmetric) [65]	johnson [70]	Stau (Stuart's tau) [71]	GW (Gilbert and Wells coefficient) [72]
disper (Dispersion) [73]	michael (Michael's coefficient of association) [74]	steffensen [75]	hellinger (Hellinger distance) [76]
DK (Driver and Kroeber) [77]	MK (Maron and Kuhns) [78]	tarantula [79], [80]	kulczynski [81]

fager [82]	mountford [83]	tarwid [84]	meanman (Canberra) [85], [86]
faith [87]	MP (Maxwell and Pilliner) [88]	tversky (Tversky feature contrast model) [89], [90]	mirkin [91]
FaMc (Fager and McGowan) [92]	ochiai [68]	UF (Upholt's F) [93]–[95]	var (Variance) [96]
FD (Forbes' D) [97]	Pcs (Pearson chi-square) [98], [99]	US (Upholt's S) [93]–[95]	
fleiss [100]	PHI (Pearson Fourfold point correlation) [101], [102]		

TABLE 2. Evaluation metrics for similarity-dissimilarity performance analysis of gray-scale-morphology-implementation.

Tag	Description
ssim	Structural similarity index measure - similarity index [103]
ms-ssim	Multiscale structural similarity index measure - similarity index [104]
peaksnr	Peak signal-to-noise ratio [105]
rmse	Root mean square error [105]

Since there will not be many variations in 1-tier morphology, the results are analyzed by applying 2-tier morphology to make the changes more evident. First of all, dilation, erosion, opening, and closing operations on binary images are applied in both domains, SIP and HIP, respectively. The SEs illustrated in Figure 2 are applied to the binary ground truth images in SIP, and those in Figure 8 are applied in the HIP domain. Figure 11 shows the similarity and dissimilarity analysis results measured during simulations. In this figure, algorithms in HIP domain and SIP domain denoted by HEX and SQ, respectively. Inherently, the similarity index between an image's original version and its processed one is desired to be low, indicating low distortion after morphology. As abovementioned, dilation operation eventually stands for edge thickening while erosion indicates edge thinning. During dilation, among the hexagonal SEs, the highest deformation occurs after the implementation of $SE_{90°\_2,\ L=5}$ and $SE_{120°,\ L=5}$ while the images are least distorted when $SE_{30°\_1,\ L=5}$ is applied. During erosion operation, the highest deformation occurs after the implementation of $SE_{150°\_2,\ L=5}$ while the images are least distorted when $SE_{0°,\ L=5}$ is applied. In SIP domain, $SE_{90°,\ L=5}$ causes the highest deformation during both dilation and erosion.

Remind that morphological closing consists of the subsequent implementation of dilation and erosion operators. In contrast, morphological opening consists of implementing erosion and dilation operators subsequently. This time, $SE_{60°,\ L=5}$ causes the highest distortion for both opening and closing operations. In SIP domain, again, $SE_{90°,\ L=5}$ causes the highest deformation during both opening and closing. Interestingly, there is a huge gap between the distortion effect of the SEs, $SE_{45°,\ L=5}$ and $SE_{135°,\ L=5}$ during dilation erosion. They do distort the image less during dilation while severely do during erosion. The exact determinations mentioned above are also valid for analyzes made on the measured grayscale morphology similarity-dissimilarity values (Tables 3-6).

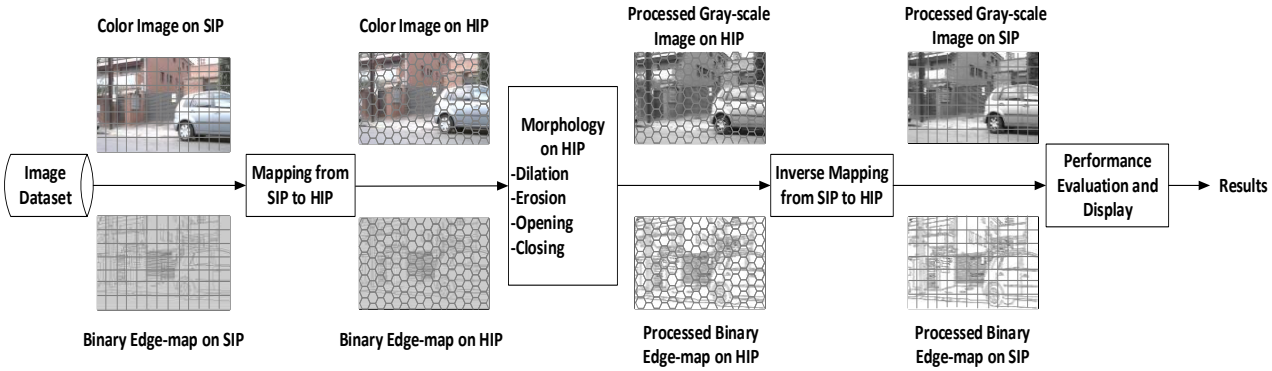

Figure 10. The illustration of the entire methodology.

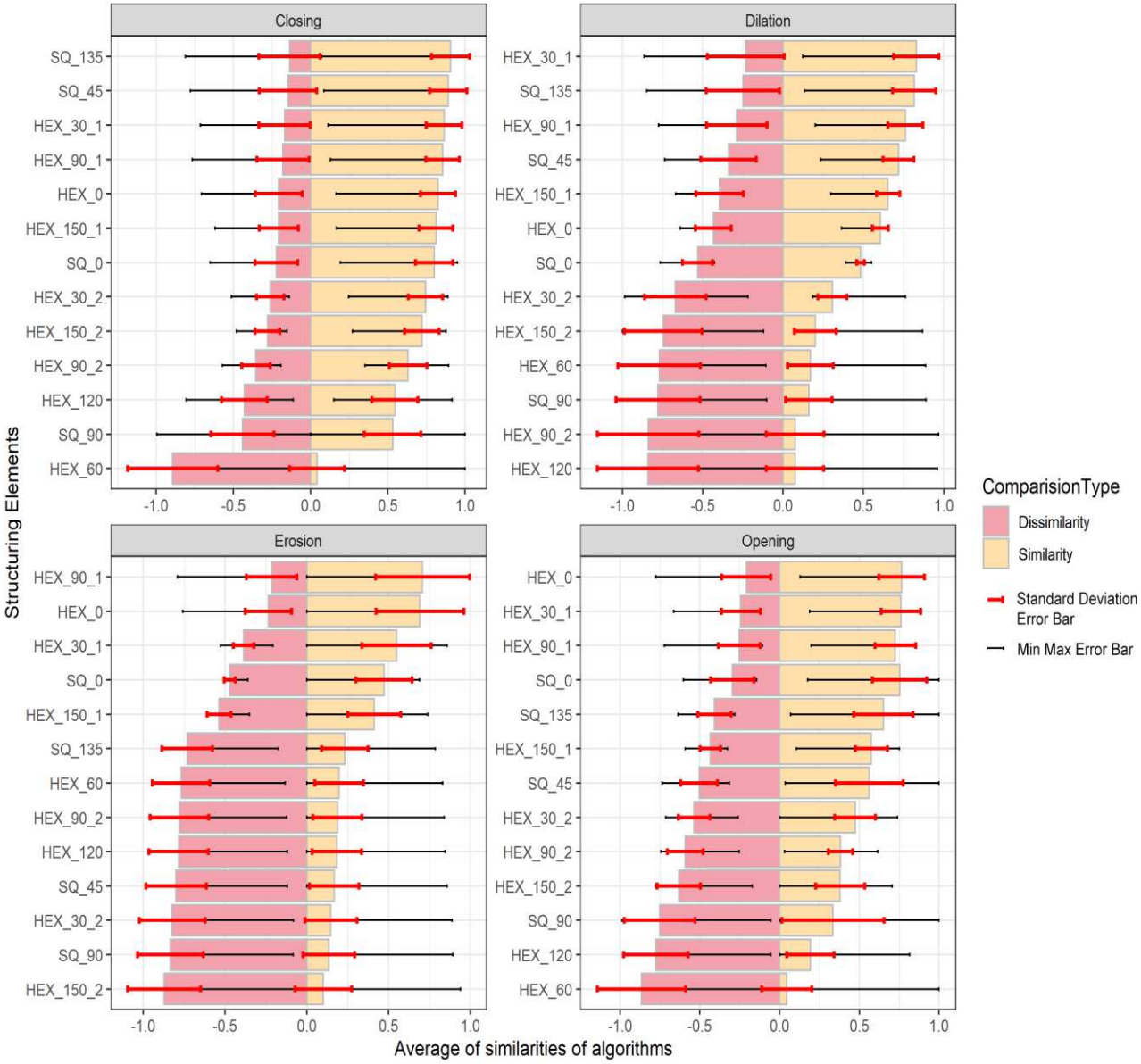

Figure 11. The similarity and dissimilarity analysis results of binary closing, dilation, erosion, and opening.

TABLE 3. The similarity and dissimilarity analysis results measured after gray-scale dilation.

	HEX_B_0_O	HEX_B_30_1_O	HEX_B_30_2_O	HEX_B_60_O	HEX_B_90_1_O	HEX_B_90_2_O	HEX_B_120_O	HEX_B_150_1_O	HEX_B_150_2_O	SQ_B_0_O	SQ_B_45_O	SQ_B_90_O	SQ_B_135_O
SSIM	0.751	0.853	0.491	0.312	0.672	0.300	0.296	0.788	0.510	0.667	0.857	0.146	0.844
PSNR	0.675	0.767	0.441	0.281	0.604	0.270	0.266	0.708	0.458	0.600	0.771	0.132	0.759
MSE	0.245	0.216	0.375	0.590	0.274	0.613	0.622	0.234	0.361	0.276	0.215	0.976	0.218

TABLE 4. The similarity and dissimilarity analysis results measured after gray-scale erosion.

	HEX_B_0_O	HEX_B_30_1_O	HEX_B_30_2_O	HEX_B_60_O	HEX_B_90_1_O	HEX_B_90_2_O	HEX_B_120_O	HEX_B_150_1_O	HEX_B_150_2_O	SQ_B_0_O	SQ_B_45_O	SQ_B_90_O	SQ_B_135_O
SSIM	0.681	0.938	0.777	0.189	0.777	0.136	0.191	0.569	0.762	0.464	0.368	0.270	0.363
PSNR	0.612	0.843	0.698	0.170	0.698	0.122	0.172	0.511	0.684	0.417	0.330	0.243	0.326
MSE	0.270	0.196	0.237	0.973	0.237	0.988	0.962	0.323	0.241	0.396	0.500	0.681	0.507

TABLE 5. The similarity and dissimilarity analysis results measured after gray-scale closing.

	HEX_B_0_O	HEX_B_30_1_O	HEX_B_30_2_O	HEX_B_60_O	HEX_B_90_1_O	HEX_B_90_2_O	HEX_B_120_O	HEX_B_150_1_O	HEX_B_150_2_O	SQ_B_0_O	SQ_B_45_O	SQ_B_90_O	SQ_B_135_O
SSIM	0.845	0.901	0.794	0.132	0.923	0.717	0.607	0.877	0.792	0.839	0.992	0.595	0.994
PSNR	0.759	0.809	0.713	0.119	0.829	0.644	0.545	0.788	0.711	0.754	0.891	0.535	0.893
MSE	0.218	0.205	0.232	0.991	0.200	0.257	0.303	0.210	0.233	0.220	0.186	0.309	0.185

TABLE 6. The similarity and dissimilarity analysis results measured after gray-scale opening.

	HEX_B_0_O	HEX_B_30_1_O	HEX_B_30_2_O	HEX_B_60_O	HEX_B_90_1_O	HEX_B_90_2_O	HEX_B_120_O	HEX_B_150_1_O	HEX_B_150_2_O	SQ_B_0_O	SQ_B_45_O	SQ_B_90_O	SQ_B_135_O
SSIM	0.811	0.882	0.589	0.236	0.784	0.396	0.247	0.807	0.572	0.780	0.654	0.258	0.658
PSNR	0.729	0.793	0.530	0.212	0.704	0.356	0.222	0.725	0.514	0.701	0.588	0.232	0.591
MSE	0.227	0.209	0.313	0.780	0.235	0.465	0.744	0.228	0.322	0.236	0.282	0.714	0.280

As an alternative, similarity analysis between an original image and its SIP, HIP-morphology-implemented versions is conducted by histogram-similarity comparison. After applying a process to an image, histogram-similarity-analysis provides essential information about how much the original deviates from its original version. During histogram-similarity-analysis on grayscale images, five metrics [106] (Correlation, Spearman, Kullback-Leibler-divergence, Chi-square-statistic, Histogram intersection, and Quadratic form distance statistics) were taken into account. The measured values for these measures drop as the deterioration following morphological treatment increases. The most severe image degradation occurs after applying morphology using the HIP domain's HEX_GS_30_1, HEX_GS_150_1 operator, and the SIP domain's SQ_GS_45, SQ_GS_90 operators; because these operators work on hexels in mid-directions in the HIP domain, but in the SIP domain, they work on pixels in diagonal directions. Hexels and pixels in the directions mentioned above have more details than others; hence, changing their intensity causes more distortion. Tables 11 and 12 show the histogram-similarity-and-dissimilarity-analysis-results measured after grayscale dilation, erosion, closing, and opening operations implemented on both SIP and HIP domains.

TABLE 11. The histogram-similarity-and-dissimilarity-analysis-results measured after gray-scale dilation and erosion.

	Correlation	Spearman	Kullback_leibler_divergence	Chi_square_statistics	Histogram_intersection	Q_F_S
HEX_GS_0_D	0.1452	0.0138	16422	5713	0.2083	7459
HEX_GS_30_1_D	0.1052	0.0162	12127	4532	0.1821	6505
HEX_GS_30_2_D	0.2000	0.0249	23221	7564	0.2471	8602
HEX_GS_60_D	0.1822	0.0190	22003	7349	0.2391	8294
HEX_GS_90_1_D	0.1090	0.0098	13130	4768	0.1900	6652
HEX_GS_90_2_D	0.2122	0.0220	25472	8208	0.2566	8840
HEX_GS_120_D	0.1782	0.0197	21493	7360	0.2377	8227
HEX_GS_150_1_D	0.1021	0.0160	12025	4574	0.1807	6444
HEX_GS_150_2_D	0.1968	0.0246	22760	7546	0.2451	8544
SQ_GS_0_D	0.1507	0.0256	Inf	6084	0.2139	7593
SQ_GS_45_D	0.1019	0.0038	11949	4487	0.1819	6437
SQ_GS_90_D	0.1831	0.0133	Inf	7486	0.2401	8312
SQ_GS_135_D	0.1062	0.0035	12325	4545	0.1839	6539
HEX_GS_0_E	0.1141	0.0625	Inf	5767	0.2404	9723
HEX_GS_30_1_E	0.1052	0.0162	12127	4532	0.1821	6505
HEX_GS_30_2_E	0.1640	0.1811	Inf	9069	0.2995	12426
HEX_GS_60_E	0.1266	0.1651	Inf	7675	0.2789	11047
HEX_GS_90_1_E	0.1090	0.0098	13130	4768	0.1900	6652
HEX_GS_90_2_E	0.1713	0.1440	Inf	9316	0.3148	12932
HEX_GS_120_E	0.1259	0.1700	Inf	7747	0.2780	11030
HEX_GS_150_1_E	0.0588	0.1214	Inf	4504	0.1943	7357
HEX_GS_150_2_E	0.1600	0.1824	Inf	9053	0.2986	12333
SQ_GS_0_E	0.1147	0.1477	Inf	6187	0.2477	9914
SQ_GS_45_E	0.0581	0.1270	Inf	4710	0.1952	7370
SQ_GS_90_E	0.1264	0.1021	Inf	7600	0.2821	11081
SQ_GS_135_E	0.0608	0.1415	Inf	4767	0.1985	7497

TABLE 11. The histogram-similarity-and-dissimilarity-analysis-results measured after gray-scale closing and opening.

	Correlation	Spearman	Kullback_leibler_divergence	Chi_square_statistics	Histogram_intersection	Q_F_S
HEX_GS_0_C	0.1141	0.0625	Inf	5767	0.2404	9723
HEX_GS_30_1_C	0.0621	0.0980	Inf	4450	0.1969	7463
HEX_GS_30_2_C	0.1640	0.1811	Inf	9069	0.2995	12426
HEX_GS_60_C	0.1266	0.1651	Inf	7675	0.2789	11047
HEX_GS_90_1_C	0.0638	0.0610	Inf	4145	0.2015	7613
HEX_GS_90_2_C	0.1713	0.1440	Inf	9316	0.3148	12932
HEX_GS_120_C	0.1259	0.1700	Inf	7747	0.2780	11030
HEX_GS_150_1_C	0.0588	0.1214	Inf	4504	0.1943	7357
HEX_GS_150_2_C	0.1600	0.1824	Inf	9053	0.2986	12333
SQ_GS_0_C	0.0767	0.0220	Inf	2760	0.1366	5496
SQ_GS_45_C	0.0479	0.0010	4639	1785	0.1063	4374
SQ_GS_90_C	0.0998	0.0149	Inf	3562	0.1597	6227
SQ_GS_135_C	0.0488	0.0008	4690	1808	0.1091	4415
HEX_GS_0_O	0.0329	0.0422	Inf	1550	0.1170	4730
HEX_GS_30_1_O	0.0145	0.0468	Inf	1298	0.0912	3485
HEX_GS_30_2_O	0.0408	0.0719	Inf	2379	0.1354	5571
HEX_GS_60_O	0.0282	0.1649	Inf	2196	0.1287	5269
HEX_GS_90_1_O	0.0125	0.0842	Inf	1314	0.1007	3537
HEX_GS_90_2_O	0.0459	0.1353	Inf	2724	0.1558	6318
HEX_GS_120_O	0.0377	0.1693	Inf	2767	0.1483	5762
HEX_GS_150_1_O	0.0117	0.0482	Inf	1288	0.0904	3276
HEX_GS_150_2_O	0.0365	0.0790	Inf	2266	0.1309	5332
SQ_GS_0_O	0.0330	0.1203	Inf	1929	0.1228	4959
SQ_GS_45_O	0.0116	0.1271	Inf	1769	0.0959	3399
SQ_GS_90_O	0.0378	0.0980	Inf	3049	0.1540	6132
SQ_GS_135_O	0.0137	0.1410	Inf	1822	0.0976	3561

Figures 12, 13, 14, 15 show how an image's histogram evolves following dilation, erosion, closing, and opening operations applied in the SIP and HIP domains, respectively, to better represent similarity and dissimilarity analysis via histograms.

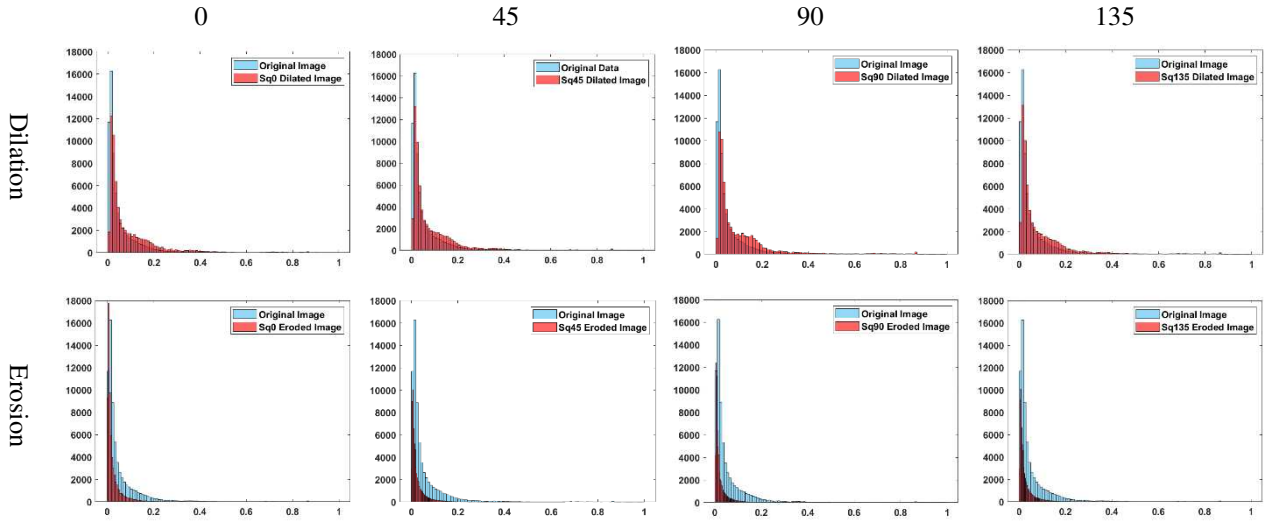

Fig. 12. Changes in the histogram after dilation and erosion operations implemented in the SIP domain.

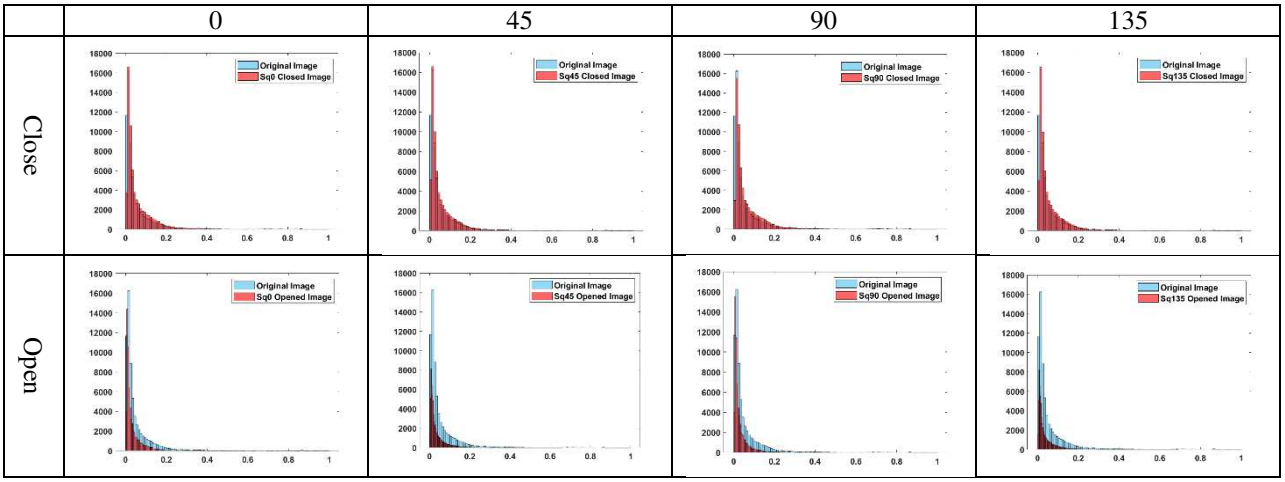

Fig. 13. Changes in the histogram after closing and opening operations implemented in the SIP domain.

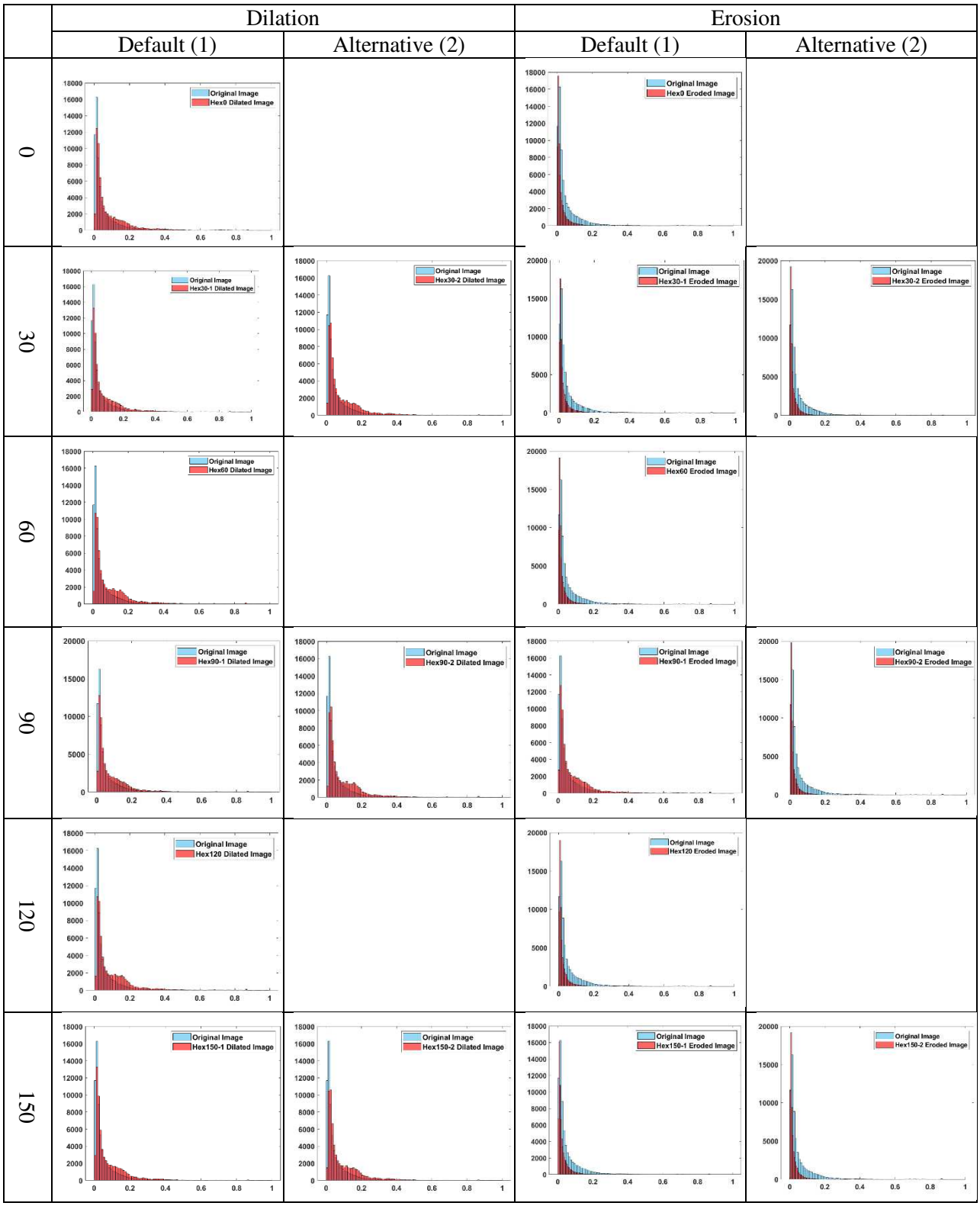

Fig. 14. Changes in the histogram after dilation and erosion operations implemented in the HIP domain.

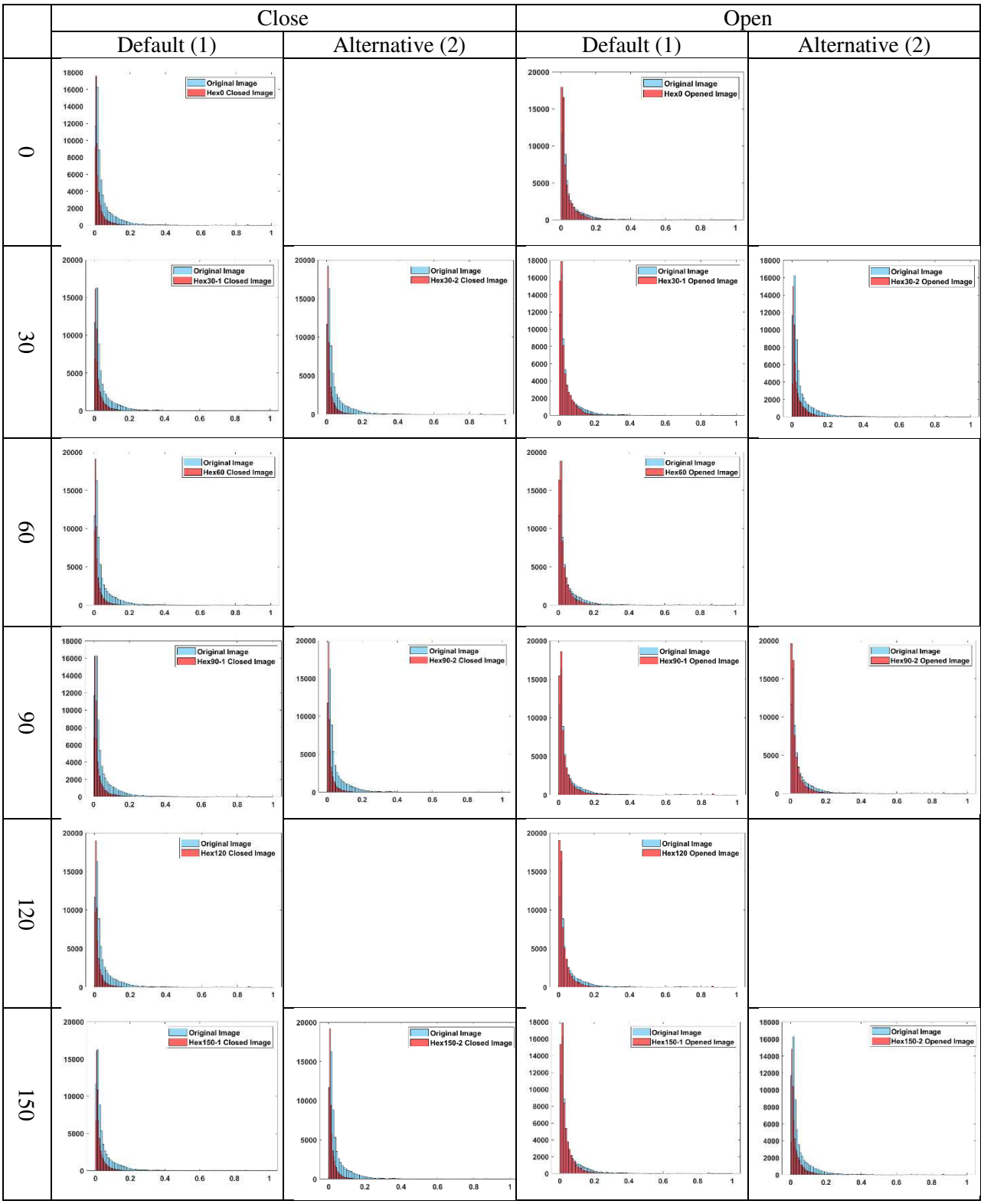

Fig. 15. Changes in the histogram after closing and opening operations implemented in the HIP domain.

6. Conclusion

In image processing, for binary and grayscale images, morphological operators are commonly used to eliminate noise, recognize contours or specific structures, and arrange shapes. Although morphology has been substantially developed in SIP, no effort has been made to construct morphological operators in the hexagonal domain -HIP- yet. In this paper, we transform basic SIP-domain-morphological operators such as dilation, erosion, closing, and opening into HIP-domain and compare their performance with their SIP counterparts in terms of the level of distortion occurring on the images after the process. Comprehensive simulations are conducted to measure distortion that arises after the operations, dilation, erosion, opening, and closing. The level of distortion is measured by considering the maintained similarity between the original images and those of their morphologically processed versions. While investigating how the morphology works in the HIP, both the binary and grayscale implementations are discussed. The results of our extensive simulations, the proposed HIP morphological operators work successfully and fill a significant gap by eliminating the lack of basic morphology operators in the HIP. Complementing this significant step is achieved by presenting the HIP equivalence of one of the major constituents of the image processing. After successfully implementing the basic morphology operators in the HIP domain, we are considering moving towards performing more complex operations using these operators in image processing in the HIP domain.

References

[1] T. Cevik, M. Fettahoglu, N. Cevik, and S. Yilmaz, "FTSH: a framework for transition from square image processing to hexagonal image processing," *Multimedia Tools and Applications*, vol. 79, no. 11–12, pp. 7021–7048, Mar. 2020, doi: 10.1007/S11042-019-08487-Z/TABLES/2.

[2] T. Hales, "Cannonballs and honeycombs," *Notices of the AMS*, vol. 47, no. 4, pp. 440–449, 2000.

[3] T. Hales, "The honeycomb conjecture," *Discrete & Computational Geometry*, vol. 25, no. 1, pp. 1–22, 2001.

[4] S. Coleman, B. Scotney, and B. Gardiner, "Processing Hexagonal Images in a Virtual Environment," *Lecture Notes in Computer Science (including subseries Lecture Notes in Artificial Intelligence and Lecture Notes in Bioinformatics)*, vol. 5716 LNCS, pp. 920–928, 2009, doi: 10.1007/978-3-642-04146-4_98.

[5] J. D. Allen, "Perfect reconstruction filter banks for the hexagon grid," *2005 Fifth International Conference on Information, Communications and Signal Processing*, vol. 2005, pp. 73–76, 2005, doi: 10.1109/ICICS.2005.1689007.

[6] J. G. Postaire, R. D. Zhang, and C. Lecocq-Botte, "Cluster Analysis by Binary Morphology," *IEEE Transactions on Pattern Analysis and Machine Intelligence*, vol. 15, no. 2, pp. 170–180, 1993, doi: 10.1109/34.192490.

[7] J. Debayle and J. C. Pinoli, "Multiscale image filtering and segmentation by means of adaptive neighborhood mathematical morphology," *Proceedings - International Conference on Image Processing, ICIP*, vol. 3, pp. 537–540, 2005, doi: 10.1109/ICIP.2005.1530447.

[8] S. R. Sternberg, "Industrial Morphology," *https://doi.org/10.1117/12.944864*, vol. 0504, pp. 202–215, Dec. 1984, doi: 10.1117/12.944864.

[9] F. Y. Shih and O. R. Mitchell, "Skeletonization And Distance Transformation By Greyscale Morphology," *Automated Inspection and High-Speed Vision Architectures*, vol. 0849, p. 80, Mar. 1988, doi: 10.1117/12.942827.

[10] F. Y. Shih and O. R. Mitchell, "Automated fast recognition and location of arbitrarily shaped objects by image morphology.," pp. 774–779, 1988, doi: 10.1109/CVPR.1988.196322.

[11] S. R. Sternberg, "Biomedical Image Processing," *Computer*, vol. 16, no. 1, pp. 22–34, 1983, doi: 10.1109/MC.1983.1654163.

[12] F. Y. Shih and O. R. Mitchell, "INDUSTRIAL PARTS RECOGNITION AND INSPECTION BY IMAGE MORPHOLOGY.," pp. 1764–1766, 1988, doi: 10.1109/ROBOT.1988.12321.

[13] M. Bastir *et al.*, "Workflows in a virtual morphology lab: 3D scanning, measuring, and printing," *Journal of Anthropological Sciences*, vol. 97, pp. 107–134, 2019, doi: 10.4436/JASS.97003.
[14] C. C. Pu and F. Y. Shih, "Threshold Decomposition of Gray-Scale Soft Morphology into Binary Soft Morphology," *Graphical Models and Image Processing*, vol. 57, no. 6, pp. 522–526, Nov. 1995, doi: 10.1006/GMIP.1995.1042.
[15] S. R. Sternberg, "A morphological approach to finished surface inspection," *Proceedings - IEEE International Conference on Robotics and Automation*, pp. 462–465, 1985, doi: 10.1109/ROBOT.1985.1087252.
[16] G. (Georges) Matheron, *Random sets and integral geometry*. New York [etc.]: J. Wiley & Sons, 1975.
[17] J. Paul. Serra, "Image analysis and mathematical morphology," 1982.
[18] J. Serra, "Image Analysis and Mathematical Morphology, Vol. 2: Theoretical Advances," Feb. 1988, Accessed: Mar. 29, 2022. [Online]. Available: citeulike-article-id:7544267
[19] C. R. (Charles R. Giardina and E. R. Dougherty, "Morphological methods in image and signal processing," p. 321, 1988.
[20] R. M. Haralick, S. R. Sternberg, and X. Zhuang, "Image Analysis Using Mathematical Morphology," *IEEE Transactions on Pattern Analysis and Machine Intelligence*, vol. PAMI-9, no. 4, pp. 532–550, 1987, doi: 10.1109/TPAMI.1987.4767941.
[21] P. Maragos, "Tutorial On Advances In Morphological Image Processing And Analysis," *https://doi.org/10.1117/12.937249*, vol. 0707, pp. 64–74, Nov. 1986, doi: 10.1117/12.937249.
[22] S. R. Sternberg, "Cellular Computers and Biomedical Image Processing," pp. 294–319, 1982, doi: 10.1007/978-3-642-93218-2_27.
[23] S. R. Sternberg, "Grayscale morphology," *Computer Vision, Graphics, and Image Processing*, vol. 35, no. 3, pp. 333–355, Sep. 1986, doi: 10.1016/0734-189X(86)90004-6.
[24] X. He and W. Jia, "Hexagonal structure for intelligent vision," *Proceedings of 1st International Conference on Information and Communication Technology, ICICT 2005*, vol. 2005, pp. 52–64, 2005, doi: 10.1109/ICICT.2005.1598543.
[25] O. R. Mitchell, "A Mathematical Morphology Approach to Euclidean Distance Transformation," *IEEE Transactions on Image Processing*, vol. 1, no. 2, pp. 197–204, 1992, doi: 10.1109/83.136596.
[26] A. Haas, G. Matheron, and J. Serra, "Morphologie mathematique et granulometries en place".
[27] F. Y. Shih, *Image processing and mathematical morphology : fundamentals and applications*. CRC Press, 2009. Accessed: Mar. 29, 2022. [Online]. Available: https://www.routledge.com/Image-Processing-and-Mathematical-Morphology-Fundamentals-and-Applications/Shih/p/book/9781138112285
[28] Y. Nakagawa and A. Rosenfeld, "A note on the use of local min and max operations in digital picture processing," *IEEE Transactions on Systems, Man and Cybernetics*, vol. 8, no. 8, pp. 632–635, 1978, doi: 10.1109/TSMC.1978.4310040.
[29] F. G. B. de Natale and G. Boato, "Detecting Morphological Filtering of Binary Images," *IEEE Transactions on Information Forensics and Security*, vol. 12, no. 5, pp. 1207–1217, May 2017, doi: 10.1109/TIFS.2017.2656472.
[30] J. D. Trivedi, S. D. Mandalapu, and D. H. Dave, "Vision-based real-time vehicle detection and vehicle speed measurement using morphology and binary logical operation," *Journal of Industrial Information Integration*, p. 100280, Sep. 2021, doi: 10.1016/J.JII.2021.100280.
[31] K. Parvati, B. S. Prakasa Rao, and M. Mariya Das, "Image segmentation using gray-scale morphology and marker-controlled watershed transformation," *Discrete Dynamics in Nature and Society*, vol. 2008, 2008, doi: 10.1155/2008/384346.
[32] O. Déforges, N. Normand, and M. Babel, "Fast recursive grayscale morphology operators: From the algorithm to the pipeline architecture," *Journal of Real-Time Image Processing*, vol. 8, no. 2, pp. 143–152, Jun. 2013, doi: 10.1007/S11554-010-0171-8/TABLES/1.
[33] X. Soria, E. Riba, and A. Sappa, "Dense Extreme Inception Network: Towards a Robust CNN Model for Edge Detection," *2020 IEEE Winter Conference on Applications of Computer Vision (WACV)*, pp. 1912–1921, Mar. 2020, doi: 10.1109/WACV45572.2020.9093290.

[34] "simbin(mat1,mat2,type,mask) - File Exchange - MATLAB Central." Accessed: Mar. 29, 2022. [Online]. Available: https://www.mathworks.com/matlabcentral/fileexchange/55190-simbin-mat1-mat2-type-mask

[35] M. R. (Michael R. Anderberg, *Cluster analysis for applications*. Academic Press, 1973.

[36] Air Force Office of Scientific Research, "Optimization and Standardization of Information Retrieval Language and Systems," 1966. Accessed: Mar. 30, 2022. [Online]. Available: https://books.google.com.tr/books/about/Optimization_and_Standardization_of_Info.html?id=9McrAQAAMAAJ&redir_esc=y

[37] S. Glen, "Correlation Coefficient: Simple Definition, Formula, Easy Calculation Steps," *StatisticsHowTo.com*. https://www.statisticshowto.com/probability-and-statistics/correlation-coefficient-formula/ (accessed Mar. 30, 2022).

[38] W. J. Conover, *Practical Nonparametric Statistics*, 3rd ed. Wiley, 1999. Accessed: Mar. 30, 2022. [Online]. Available: https://www.wiley.com/en-us/Practical+Nonparametric+Statistics%2C+3rd+Edition-p-9780471160687

[39] C. Kurtz, A. Depeursinge, S. Napel, C. F. Beaulieu, and D. L. Rubin, "On combining image-based and ontological semantic dissimilarities for medical image retrieval applications," *Medical Image Analysis*, vol. 18, no. 7, pp. 1082–1100, Oct. 2014, doi: 10.1016/J.MEDIA.2014.06.009.

[40] V. Dallmeier, C. Lindig, and A. Zeller, *Lightweight Defect Localization for Java*, vol. 3586. Springer, Berlin, Heidelberg, 2005. doi: 10.1007/11531142_23.

[41] C. Gini, "Measurement of Inequality of Incomes," *The Economic Journal*, vol. 31, no. 121, pp. 124–126, 1921, Accessed: Mar. 30, 2022. [Online]. Available: https://www.jstor.org/stable/pdf/2223319.pdf

[42] D. J. Rogers and T. T. Tanimoto, "A computer program for classifying plants," *Science*, vol. 132, no. 3434, pp. 1115–1118, Oct. 1960, doi: 10.1126/SCIENCE.132.3434.1115/ASSET/533027DC-D370-4581-A81B-4ABEE1FDFFBA/ASSETS/SCIENCE.132.3434.1115.FP.PNG.

[43] S. Choi and S. Cha, "A survey of Binary similarity and distance measures," *JOURNAL OF SYSTEMICS, CYBERNETICS AND INFORMATICS*, vol. 8, no. 1, pp. 43--48, 2010, Accessed: Mar. 30, 2022. [Online]. Available: http://citeseerx.ist.psu.edu/viewdoc/summary?doi=10.1.1.352.6123

[44] J. Braun-Blanquet, J. Braun-Blanquet, H. S. Conard, and G. D. Fuller, *Plant sociology; the study of plant communities*, 1st ed. New York and London,: McGraw-Hill book company, inc., 1932. doi: 10.5962/bhl.title.7161.

[45] L. A. Goodman and W. H. Kruskal, "Measures of Association for Cross Classifications," *Journal of the American Statistical Association*, vol. 49, no. 268, p. 732, Dec. 1954, doi: 10.2307/2281536.

[46] L. A. Goodman and W. H. Kruskal, "Measures of Association for Cross Classifications. II: Further Discussion and References," *Journal of the American Statistical Association*, vol. 54, no. 285, pp. 123–163, 1959, doi: 10.1080/01621459.1959.10501503.

[47] L. A. Goodman and W. H. Kruskal, "Measures of Association for Cross Classifications III: Approximate Sampling Theory," *Journal of the American Statistical Association*, vol. 58, no. 302, pp. 310–364, 1963, doi: 10.1080/01621459.1963.10500850.

[48] L. A. Goodman and W. H. Kruskal, "Measures of association for cross classifications, IV: Simplification of asymptotic variances," *Journal of the American Statistical Association*, vol. 67, no. 338, pp. 415–421, 1972, doi: 10.1080/01621459.1972.10482401.

[49] W. A. Scott, "Reliability of content analysis: The case of nominal scale coding," *Public Opinion Quarterly*, vol. 19, no. 3, pp. 321–325, Sep. 1955, doi: 10.1086/266577.

[50] G. N. Lance and W. T. Williams, "A general theory of classificatory sorting strategies: II. Clustering systems," *The Computer Journal*, vol. 10, no. 3, pp. 271–277, Mar. 1967, doi: 10.1093/COMJNL/10.3.271.

[51] C. Baroni-Urbani and M. W. Buser, "Similarity of Binary Data," *Systematic Biology*, vol. 25, no. 3, pp. 251–259, Sep. 1976, doi: 10.2307/2412493.

[52] R. Sokal, *A statistical method for evaluating systematic relationships*. Lawrence, Kan. : University of Kansas, 1958.

[53] "Distances Similarity Measures for Binary Data," *SPSS Statistics 28.0.0 - IBM Documentation*. https://www.ibm.com/docs/en/spss-statistics/28.0.0 (accessed Mar. 30, 2022).
[54] L. Vergni, F. Todisco, and B. di Lena, "Evaluation of the similarity between drought indices by correlation analysis and Cohen's Kappa test in a Mediterranean area," *Natural Hazards*, vol. 108, no. 2, pp. 2187–2209, Sep. 2021, doi: 10.1007/S11069-021-04775-W.
[55] J. W. Goodall, "The distribution of the simple matching coefficient," *Biometrics*, vol. 23, pp. 647–656, 1967, Accessed: Mar. 30, 2022. [Online]. Available: https://www.osti.gov/servlets/purl/7107246
[56] R. Ehsani and F. Drabløs, "Robust Distance Measures for kNN Classification of Cancer Data.," *Cancer informatics*, vol. 19, p. 1176935120965542, Oct. 2020, doi: 10.1177/1176935120965542.
[57] É. Baudrier, F. Nicolier, G. Millon, and S. Ruan, "Binary-image comparison with local-dissimilarity quantification," *Pattern Recognition*, vol. 41, no. 5, pp. 1461–1478, May 2008, doi: 10.1016/J.PATCOG.2007.07.011.
[58] L. C. Cole, "The Measurement of Interspecific Associaton," *Ecology*, vol. 30, no. 4, pp. 411–424, Oct. 1949, doi: 10.2307/1932444.
[59] H. U. Merkmalbestand, *Verwandschaftsbeziehungen der Farinosae, Ein Beitrag zum System der Monokotyledonen*, vol. 2. Willdenowia, 1961. Accessed: Mar. 30, 2022. [Online]. Available: https://www.zobodat.at/pdf/MON-B_0043_0001-0765.pdf
[60] T. Sørensen, *A method of establishing groups of equal amplitude in plant sociology based on similarity of species content and its application to analyses of the vegetation on Danish commons.*, vol. 5. København, I kommission hos E. Munksgaard, 1948.
[61] J. Guiot, "Methodology of the last climatic cycle reconstruction in France from pollen data," *Palaeogeography, Palaeoclimatology, Palaeoecology*, vol. 80, no. 1, pp. 49–69, Sep. 1990, doi: 10.1016/0031-0182(90)90033-4.
[62] D. MAYNES, "Detection of Non-Independent Test Taking by Similarity Analysis | DENN," in *Test Fraud*, Taylor & Francis, 2014, pp. 53–82. Accessed: Mar. 30, 2022. [Online]. Available: https://www.taylorfrancis.com/chapters/edit/10.4324/9781315884677-12/detection-non-independent-test-taking-similarity-analysis-dennis-maynes
[63] R. P. Hawkins and V. A. Dotson, "Reliability scores that delude: An Alice in Wonderful trip through the misleading characteristics of interobserver agreement scores in interval coding. In Ramp E. & Semb G. (Eds.), Behavior analysis: areas of research and application," 1968.
[64] T. Sorgenfrei, "Molluscan Assemblages from the Marine Middle Miocene of South Jutland and their Environments. Vol. I.," *Danmarks Geologiske Undersøgelse II. Række*, vol. 79, pp. 1–355, Dec. 1958, doi: 10.34194/RAEKKE2.V79.6868.
[65] L. R. Dice, "Measures of the Amount of Ecologic Association Between Species," *Ecology*, vol. 26, no. 3, pp. 297–302, Jul. 1945, doi: 10.2307/1932409.
[66] P. Jaccard, "THE DISTRIBUTION OF THE FLORA IN THE ALPINE ZONE.1," *New Phytologist*, vol. 11, no. 2, pp. 37–50, Feb. 1912, doi: 10.1111/J.1469-8137.1912.TB05611.X.
[67] T. T. Tanimoto, *An elementary mathematical theory of classification and prediction*. Internal IBM Technical Report, 1958. Accessed: Mar. 30, 2022. [Online]. Available: https://catalogue.nla.gov.au/Record/1717218
[68] A. Ochiai, "Zoogeographical Studies on the Soleoid Fishes Found in Japan and its Neighhouring Regions-II," *Bulletin of the Japanese Society of Scientific Fisheries*, vol. 22, no. 9, pp. 526–530, Jan. 1957, doi: 10.2331/SUISAN.22.526.
[69] H. H. Ross, "Principles of Numerical Taxonomy," *Systematic Biology*, vol. 13, no. 1–4, pp. 106–108, Mar. 1964, doi: 10.2307/SYSBIO/13.1-4.106.
[70] S. C. Johnson, "Hierarchical clustering schemes," *Psychometrika 1967 32:3*, vol. 32, no. 3, pp. 241–254, Sep. 1967, doi: 10.1007/BF02289588.
[71] A. Stuart, "The Estimation and Comparison of Strengths of Association in Contingency Tables," *Biometrika*, vol. 40, no. 1/2, p. 105, Jun. 1953, doi: 10.2307/2333101.
[72] N. Gilbert and T. C. E. Wells, "Analysis of Quadrat Data," *The Journal of Ecology*, vol. 54, no. 3, p. 675, Nov. 1966, doi: 10.2307/2257810.

[73] D. R. Cox, *The Statistical Analysis of Series of Events.* Springer Verlag, 2014. Accessed: Mar. 30, 2022. [Online]. Available: https://link.springer.com/book/9789401178037
[74] E. L. Michael, "Marine Ecology and the Coefficient of Association: A Plea in Behalf of Quantitative Biology," *The Journal of Ecology*, vol. 8, no. 1, p. 54, Mar. 1920, doi: 10.2307/2255213.
[75] F. N. David, "Biometrika," *Oxford University Press*, vol. 26, no. 1/2, p. 1, May 1934, doi: 10.2307/2332052.
[76] E. Hellinger, "Neue Begründung der Theorie quadratischer Formen von unendlichvielen Veränderlichen," *Journal fur die Reine und Angewandte Mathematik*, vol. 1909, no. 136, pp. 210–271, Jul. 1909, doi: 10.1515/CRLL.1909.136.210/MACHINEREADABLECITATION/RIS.
[77] H. Driver and A. L. Kroeber, *Quantitative expression of cultural relationships*. Berkeley: University of California Press, 1932.
[78] P. Thompson, "Looking back: On relevance, probabilistic indexing and information retrieval," *Information Processing & Management*, vol. 44, no. 2, pp. 963–970, Mar. 2008, doi: 10.1016/J.IPM.2007.10.002.
[79] J. A. Jones and M. J. Harrold, "Empirical evaluation of the tarantula automatic fault-localization technique," *20th IEEE/ACM International Conference on Automated Software Engineering, ASE 2005*, pp. 273–282, 2005, doi: 10.1145/1101908.1101949.
[80] M. Brusco, J. Dennis Cradit, and D. Steinley, "A comparison of 71 binary similarity coefficients: The effect of base rates," *PLOS ONE*, vol. 16, no. 4, p. e0247751, Apr. 2021, doi: 10.1371/JOURNAL.PONE.0247751.
[81] S. Kulczyński, "Die Pflanzenassoziationen der Pieninen," *Bulletin de l'Académie polonaise des sciences. Série des sciences biologiques*, 1928.
[82] E. W. Fager, "Determination and Analysis of Recurrent Groups," *Ecology*, vol. 38, no. 4, pp. 586–595, Oct. 1957, doi: 10.2307/1943124.
[83] M. D. Mountford, "An index of similarity and its application to classification problems," *Progress in Soil Zoology*, pp. 43–50, 1962.
[84] S. H. Wijaya, F. M. Afendi, I. Batubara, L. K. Darusman, M. Altaf-Ul-Amin, and S. Kanaya, "Finding an appropriate equation to measure similarity between binary vectors: Case studies on Indonesian and Japanese herbal medicines," *BMC Bioinformatics*, vol. 17, no. 1, pp. 1–19, Dec. 2016, doi: 10.1186/S12859-016-1392-Z/FIGURES/6.
[85] G. N. Lance and W. T. Williams, "Computer Programs for Hierarchical Polythetic Classification ('Similarity Analyses')," *The Computer Journal*, vol. 9, no. 1, pp. 60–64, May 1966, doi: 10.1093/COMJNL/9.1.60.
[86] G. Lance and W. T. Williams, "Mixed-Data Classificatory Programs I - Agglomerative Systems," *Australian Computer Journal*, pp. 15–22, 1967, Accessed: Mar. 30, 2022. [Online]. Available: https://www.semanticscholar.org/paper/Mixed-Data-Classificatory-Programs-I-Agglomerative-Lance-Williams/4072b6353dd761ba0c219a4b860073f08bb3db27
[87] D. P. Faith, "Conservation evaluation and phylogenetic diversity," *Biological Conservation*, vol. 61, no. 1, pp. 1–10, Jan. 1992, doi: 10.1016/0006-3207(92)91201-3.
[88] A. E. Maxwell and A. E. G. Pilliner, "DERIVING COEFFICIENTS OF RELIABILITY AND AGREEMENT FOR RATINGS," *British Journal of Mathematical and Statistical Psychology*, vol. 21, no. 1, pp. 105–116, May 1968, doi: 10.1111/J.2044-8317.1968.TB00401.X.
[89] A. Tversky, "Features of similarity," *Psychological Review*, vol. 84, no. 4, pp. 327–352, Jul. 1977, doi: 10.1037/0033-295X.84.4.327.
[90] D. J. Navarro and M. D. Lee, "Common and distinctive features in stimulus similarity: A modified version of the contrast model," *Psychonomic Bulletin & Review 2004 11:6*, vol. 11, no. 6, pp. 961–974, 2004, doi: 10.3758/BF03196728.
[91] B. G. MIRKIN and I. MUCHNIK, "CLUSTERING AND MULTIDIMENSIONAL SCALING IN RUSSIA (1960–1990): A REVIEW," *Clustering and Classification*, pp. 295–339, Jan. 1996, doi: 10.1142/9789812832153_0009.

[92] E. W. Fager and J. A. McGowan, "Zooplankton species groups in the North Pacific," *Science*, vol. 140, no. 3566, pp. 453–460, May 1963, doi: 10.1126/SCIENCE.140.3566.453/ASSET/63D04A31-A33A-496C-8B8D-88133CF44CDB/ASSETS/SCIENCE.140.3566.453.FP.PNG.

[93] W. B. Upholt and I. B. Dawid, "Mapping of mitochondrial DNA of individual sheep and goats: rapid evolution in the D loop region," *Cell*, vol. 11, no. 3, pp. 571–583, 1977, doi: 10.1016/0092-8674(77)90075-7.

[94] W. B. Upholt, "Estimation of DNA sequence divergence from comparison of restriction endonuclease digests.," *Nucleic Acids Research*, vol. 4, no. 5, p. 1257, Jun. 1977, doi: 10.1093/NAR/4.5.1257.

[95] J. C. Avise, *Molecular Markers, Natural History and Evolution*. Springer US, 1994. doi: 10.1007/978-1-4615-2381-9.

[96] L. Wasserman, *All of statistics : a concise course in statistical inference*. Springer, 2004.

[97] S. A. Forbes, "On the Local Distribution of Certain Illinois Fishes:," *Illinois Natural History Survey Bulletin*, vol. 7, no. 1–10, pp. 273–303, Apr. 1909, doi: 10.21900/J.INHS.V7.407.

[98] K. Pearson, "On the criterion that a given system of deviations from the probable in the case of a correlated system of variables is such that it can be reasonably supposed to have arisen from random sampling," *The London, Edinburgh, and Dublin Philosophical Magazine and Journal of Science*, vol. 50, no. 302, pp. 157–175, Jul. 1900, doi: 10.1080/14786440009463897.

[99] R. A. Fisher, "On the Interpretation of χ 2 from Contingency Tables, and the Calculation of P," *Journal of the Royal Statistical Society*, vol. 85, no. 1, p. 87, Jan. 1922, doi: 10.2307/2340521.

[100] W. A. Shewart *et al.*, *Statistical Methods for Rates and Proportions*, 3rd ed. John Wiley & Sons, Inc., 2003. doi: 10.1002/0471445428.

[101] "Pearson Correlation - SPSS." Accessed: Mar. 30, 2022. [Online]. Available: https://libguides.library.kent.edu/SPSS/PearsonCorr

[102] R. A. Fisher, "The Conditions Under Which χ2 Measures the Discrepancey Between Observation and Hypothesis on JSTOR," *Journal of the Royal Statistical Society*, vol. 87, no. 3, pp. 442–450, 1924, Accessed: Mar. 30, 2022. [Online]. Available: https://www.jstor.org/stable/2341149?seq=1

[103] Z. Wang, A. C. Bovik, H. R. Sheikh, and E. P. Simoncelli, "Image quality assessment: From error visibility to structural similarity," *IEEE Transactions on Image Processing*, vol. 13, no. 4, pp. 600–612, Apr. 2004, doi: 10.1109/TIP.2003.819861.

[104] Z. Wang, E. P. Simoncelli, and A. C. Bovik, "Multi-scale structural similarity for image quality assessment," *Conference Record of the Asilomar Conference on Signals, Systems and Computers*, vol. 2, pp. 1398–1402, 2003, doi: 10.1109/ACSSC.2003.1292216.

[105] A. Boutemedjet, C. Deng, and B. Zhao, "Robust Approach for Nonuniformity Correction in Infrared Focal Plane Array," *Sensors 2016, Vol. 16, Page 1890*, vol. 16, no. 11, p. 1890, Nov. 2016, doi: 10.3390/S16111890.

[106] Y. Rubner, C. Tomasi, and L. J. Guibas, "The Earth Mover's Distance as a Metric for Image Retrieval," *International Journal of Computer Vision 2000 40:2*, vol. 40, no. 2, pp. 99–121, Nov. 2000, doi: 10.1023/A:1026543900054.